ACS Sustainable Chemistry & Engineering

pubs.acs.org/journal/ascecg

Research Article

Electrochemical Separation of Alkaline-Earth Elements from Molten Salts Using Liquid Metal Electrodes

Thomas P. Nigl, Timothy Lichtenstein, Yuran Kong, and Hojong Kim*

Cite This: https://dx.doi.org/10.1021/acssuschemeng.0c04249

Read Online

ACCESS | Metrics & More | Article Recommendations

ABSTRACT: Closing the nuclear fuel cycle requires recycling used nuclear fuel. Additional waste is generated during recycling due to fission products accumulating in processing salts (LiCl–KCl). Reducing the waste generated during recycling entails recovering alkaline-earth fission products (Ba^{2+}/Sr^{2+}) from molten chlorides with a minimal loss of bulk electrolyte constituents (Li^+/K^+). Electrochemical codeposition of Ba^{2+}/Li^+ and Sr^{2+}/Li^+ into liquid metal (Bi, Sb, Sn, and Pb) and alloy (Bi–Sb) electrodes was investigated in LiCl–KCl–($BaCl_2$, $SrCl_2$) electrolytes at 500 and 650 °C. For the pure Bi (500 °C) and Sb (650 °C) electrodes, the greatest percentage of charge was used to deposit Ba and Sr. Effective recovery of Ba/Sr by liquid Bi and Sb electrodes is supported via experimentally determined activity values of Ba/Sr in Bi and Sb. Alloying Sb with Bi increased Ba recovery but decreased Sr recovery, compared to the recovery using a liquid Bi electrode. The results suggest that alkaline-earth fission products can be recovered from molten chlorides using liquid metal electrodes via electrochemical separation, thereby providing a method to reduce the generation of nuclear waste from nuclear fuel recycling.

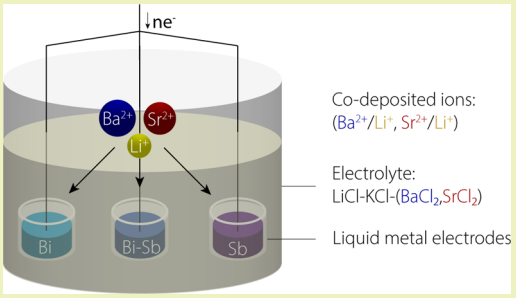

KEYWORDS: *molten salts, liquid metal electrodes, electrochemical separation, used nuclear fuel recycling, nuclear fuel cycle, electrorefining, alkaline-earth metals*

Downloaded via Thomas Nigl on September 23, 2020 at 22:38:23 (UTC).
See https://pubs.acs.org/sharingguidelines for options on how to legitimately share published articles.

INTRODUCTION

Sustainable production of low-carbon nuclear energy requires closing the nuclear fuel cycle by recycling used nuclear fuel, for example, through pyroprocessing of molten salts. The essential step in pyroprocessing is electrorefining in which uranium oxidizes out of the used fuel anode into a eutectic LiCl–KCl molten salt electrolyte at 500 °C and deposits at the cathode for recycling.[1] While uranium is separated from the used fuel, fission products (e.g., Sr and Ba), more electrochemically active than uranium, oxidize into the electrolyte but accumulate as stable dissolved ions. The accumulation of fission products not only imparts decay heat to the system, but also changes the liquidus temperature of the electrolyte, complicating thermal management of the electrorefining process.[2−4] Consequently, a portion of the processing salt (LiCl–KCl) is removed and disposed of, thereby increasing the volume of nuclear waste that can lead to health and environmental risks if not securely contained.[5] To reduce nuclear waste from pyroprocessing, fission products must be separated with minimal removal of the processing salt. Of the fission products, the separation of alkaline-earth elements is particularly challenging since alkaline-earth salts ($BaCl_2$ and $SrCl_2$) are thermodynamically more stable than the processing salt.[6] In order to recover alkaline-earths from molten salts, this work studied strongly interacting liquid metal electrodes (Sb, Bi, Sn, and Pb) into which alkaline-earth fission products (Ba and Sr) can be electrodeposited in the liquid state.

Matsumiya et al. investigated liquid Pb, Sn, and Bi metals to recover Ba and Sr from NaCl–KCl–$BaCl_2$ at 727 °C and from NaCl–KCl–$SrCl_2$ at 800 °C, respectively.[7,8] Based on the analysis of the electrolysis products, they reported that the alkaline-earth (Ba or Sr) fission products were recovered by the liquid Pb and Sn electrodes, but not by the liquid Bi electrode (e.g., < 0.1 ppm for Sr) and postulated that an enhanced recovery capability of Pb and Sn, compared to Bi, originates from an extremely low activity coefficient (γ) of alkaline-earth metals in the liquid metals, for example, $\gamma_{Ba(in\ Pb)} = 1.5 \times 10^{-9}$, $\gamma_{Ba(in\ Sn)} = 1.5 \times 10^{-10}$, and $\gamma_{Ba(in\ Bi)} = 1.0 \times 10^{-6}$ at 727 °C. In contrast, Lichtenstein et al. investigated the constant-current electrolysis of liquid Bi electrodes in ternary LiCl–KCl–$SrCl_2$/$BaCl_2$ (56.7–38.3–5 mol %) electrolytes at 500 °C and reported the substantial recovery of Ba (12 mol %) and Sr (6.5 mol %) in liquid Bi.[9] They also postulated that the unique capability of liquid Bi for alkaline-earth recovery is

Received: June 8, 2020
Revised: September 2, 2020
Published: September 10, 2020

© XXXX American Chemical Society

attributed to the extremely low γ of alkaline-earth metals in liquid Bi, for example, $\gamma_{Ba} = 1.5 \times 10^{-14}$ and $\gamma_{Sr} = 1.6 \times 10^{-12}$ at 500 °C, as determined from emf measurements.[10,11]

The comparison of results from the studies by Matsumiya et al. and Lichtenstein et al. clearly illustrates inconsistencies in the assessment of liquid Bi for alkaline-earth recovery as well as in γ_{Ba} by nine orders of magnitude, inviting scrutiny into the capability of liquid metals for alkaline-earth recovery from molten salts. Thermodynamic properties of eight binary (Ba, Sr)−(Bi, Sb, Sn, Pb) alloys were investigated via emf measurements ($\Delta\bar{G} = -2FE = RT \ln a$) using a solid CaF_2−BaF_2/SrF_2 electrolyte, as shown in Figure 1 for selected

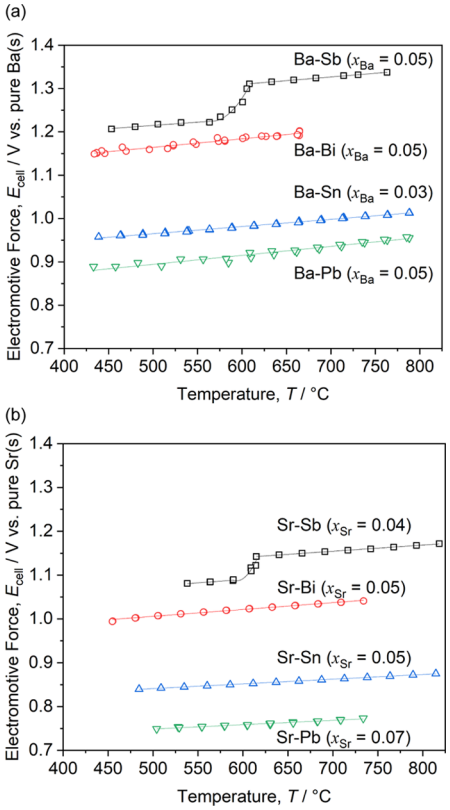
(a)
Electromotive Force, E_{cell} / V vs. pure Ba(s)
Ba-Sb (x_{Ba} = 0.05)
Ba-Bi (x_{Ba} = 0.05)
Ba-Sn (x_{Ba} = 0.03)
Ba-Pb (x_{Ba} = 0.05)
Temperature, T / °C
(b)
Electromotive Force, E_{cell} / V vs. pure Sr(s)
Sr-Sb (x_{Sr} = 0.04)
Sr-Bi (x_{Sr} = 0.05)
Sr-Sn (x_{Sr} = 0.05)
Sr-Pb (x_{Sr} = 0.07)
Temperature, T / °C

Figure 1. Emf as a function of temperature for (a) binary Ba−(Sb, Bi, Sn, Pb) alloys and (b) binary Sr−(Sb, Bi, Sn, Pb) alloys at selected mole fractions, where solid lines represent linear or curved fits.[10−17]

Ba/Sr mole fractions ($x_{Ba/Sr}$ = 0.03−0.07).[10−17] A large emf value of these liquid metals (i.e., low γ) indicates strong chemical interactions between alkaline-earth and liquid metals; the degree of interactions is strongest for Sb followed by Bi, Sn, and Pb for both Ba and Sr.

By leveraging the low γ of Ba and Sr in the liquid metals (Sb, Bi, Sn, and Pb), it is possible that liquid metal electrodes could be used to recover Ba and Sr and enable reuse of the processing salt. To evaluate the efficacy of the liquid metal electrodes in separating Ba and Sr from molten salts, liquid metals (Bi, Sb, Sn, and Pb) were subjected to constant-current (−50 mA cm^{-2}) electrolysis at 200 C g^{-1} in ternary LiCl−KCl−$BaCl_2$/$SrCl_2$ electrolytes at 500 °C, with the exception of Sb at 650 °C due to its high melting temperature ($T_{m,\,Sb}$ = 631 °C). Three liquid Bi−Sb alloys (50−50, 60−40, and 70−30 mol %) were also evaluated at 500 °C, utilizing the strong interactions of Sb and Bi with alkaline earths at a lower temperature.

EXPERIMENTAL SECTION

Electrochemical Cell Components and Assembly. All electrochemical cell components were prepared and assembled in an argon-filled glovebox (< 0.5 ppm O_2 and H_2O) to prevent the hygroscopic electrolytes and reactive electrode materials from reacting with moisture and oxygen.

Electrolytes and Electrodes. Ternary LiCl−KCl−$BaCl_2$ and LiCl−KCl−$SrCl_2$ (56.7−38.3−5.0 mol %) electrolytes were prepared from appropriate weights of pure anhydrous salts: LiCl (99.9%, Alfa Aesar), KCl (99.95%, Alfa Aesar), $SrCl_2$ (99.5%, Alfa Aesar), and $BaCl_2$ (99.998%, Alfa Aesar) by vacuum-drying and premelting at 700 °C under an Ar flow.[9] Pure liquid metal electrodes were prepared by weighing 2.7 g of pure Bi (99.999%, Sigma-Aldrich), Sb (99.999%, Alfa Aesar), Sn (99.9999%, Alfa Aesar), or Pb (99.9%, Sigma-Aldrich) pieces. Three Bi−Sb electrodes (50−50, 60−40, and 70−30 mol %) were prepared by weighing a total 2.7 g of Bi and Sb pieces. The liquid metal working electrodes (WE) were melted in a boron nitride (BN) crucible (Saint-Gobain Advanced Ceramics, Product No. AX05) using an induction heater (IH15A-2 T, Across International) custom-installed inside a glovebox. The dimensions of the BN crucible were 20 mm in height, 12 mm outer diameter, 8 mm inner diameter, and 15 mm in depth, resulting in a nominal electrode surface area of 0.5 cm^2. As the metal pieces melted during induction heating, a tungsten wire (99.95%, Thermo Shield, 1 mm diameter) was inserted into the liquid metal to establish electrical contact.

A graphite cylinder (0.95 cm diameter, 3 cm length) was used as the counter electrode (CE) in the three-electrode cells. The cylinder was female-threaded at the top and electrically connected to a male-threaded stainless steel rod. The Ag/Ag^+ reference electrode (RE) was constructed of a closed-end mullite tube (6.4 mm in outer diameter and 45.7 cm in length) filled with 0.5 g of LiCl−KCl−1 wt % AgCl electrolyte and a Ag wire (1 mm in diameter and 48.3 cm in length; 99.9%, Alfa Aesar). The LiCl−KCl−AgCl electrolyte was prepared by adding 1 wt % AgCl (anhydrous, 99.998%, Sigma-Aldrich) to eutectic LiCl−KCl and premelting the mixture using a similar procedure used to prepare the bulk electrolytes.

Cell Assembly. The electrodes and thermocouple were arranged inside an alumina crucible (60 mm in diameter and 100 mm in height; AdValue Technology). The tungsten wires and thermocouple were inserted through a stainless steel flange, electrically insulated by mullite tubes, and sealed at the top of the mullite tubes with epoxy. About 70 g of the electrolyte was poured into the crucible over the electrodes. The assembled cell was then loaded into a stainless steel vacuum chamber. The chamber was removed from the glovebox and loaded into a crucible furnace. The cell was initially heated and vacuum-dried in the chamber using a similar procedure for preparing the electrolytes, and then heated to 650 °C for the Sb electrode or 500 °C for other low-melting electrodes, and held at a temperature for 12 h to equilibrate the electrodes before measurements. The cell temperature was monitored and recorded using a data acquisition board (National Instruments, NI 9211).

Electrochemical Measurements and Characterization of Electrolysis Products. The constant-current electrolysis was conducted in a three-electrode cell. Each liquid metal WE was subjected to a constant cathodic current density (j = −50 mA cm^{-2}) up to a specific charge of 200 C g^{-1} using a potentiostat−galvanostat (Autolab PGSTAT302 N). After each electrolysis cycle, the cell was cooled to room temperature and the electrode was isolated from the system. The electrode was then separated from the BN and rinsed with deionized water to remove the entrained salt from the electrode surface. The electrode was divided into two parts: (1) for metallographic characterization, a scanning electron microscope (SEM, FEI Quanta 200) fitted with an energy dispersive X-ray spectroscope (EDS) was used and (2) for chemical analysis, an inductively coupled plasma-atomic emission spectroscope (ICP-AES, PerkinElmer Optima 5300DV) with an accuracy of 4% of the measured value was used. The metallographic sample was mounted in epoxy and dry-polished using a silicon carbide emery paper up to 1200 grit. The remaining part of the electrode was pulverized into a

https://dx.doi.org/10.1021/acssuschemeng.0c04249
ACS Sustainable Chem. Eng. XXXX, XXX, XXX−XXX

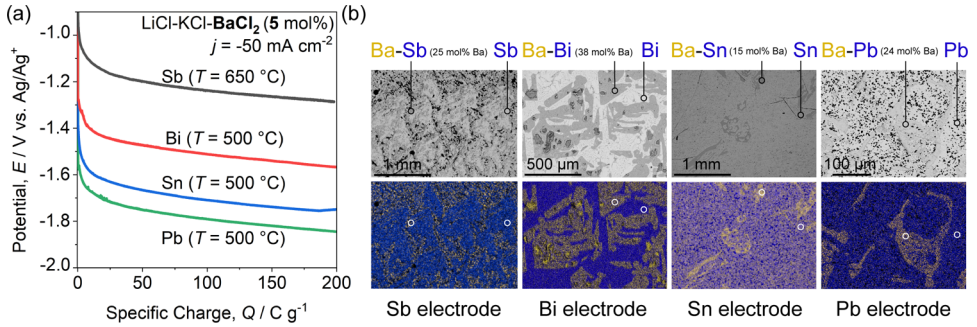

Figure 2. (a) Electrode potential of liquid metal electrodes (Sb, Bi, Sn, and Pb) during electrolysis at $j = -50$ mA cm^{-2} in LiCl–KCl–$BaCl_2$ electrolyte and (b) SEM and elemental X-ray mapping images after electrolysis at 500 or 650 °C for Sb (Ba = yellow and liquid metal = dark blue).

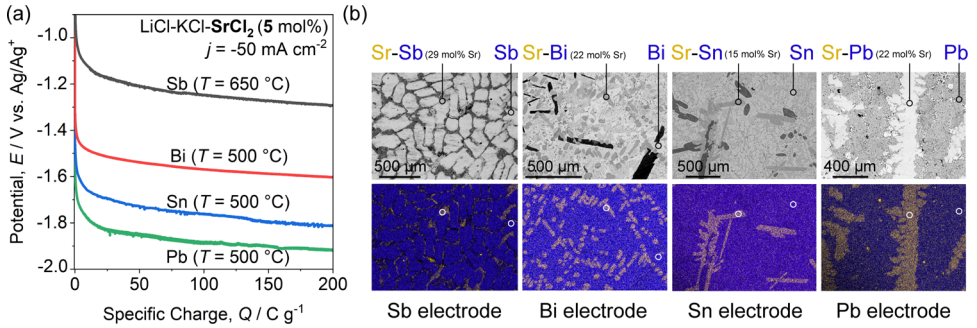

Figure 3. (a) Electrode potential of liquid metal electrodes (Sb, Bi, Sn, and Pb) during electrolysis at $j = -50$ mA cm^{-2} in LiCl–KCl–$SrCl_2$ electrolyte and (b) SEM and elemental X-ray mapping images after electrolysis at 500 or 650 °C for Sb (Sr = yellow and liquid metal = dark blue).

fine powder with a mortar and pestle in a glovebox for chemical analysis by ICP-AES.

RESULTS AND DISCUSSION

Electrolysis and Characterization of Pure Liquid Metal Electrodes. During the constant-current electrolysis at $j = -50$ mA cm^{-2}, the potential of each electrode monotonically decreased (Figures 2 and 3). The potential of the Sb electrode was the most positive followed by that of Bi, Sn, and Pb electrodes in both electrolytes, in accordance with the order of the emf results shown in Figure 1.

According to the chemical analysis by SEM–EDS, Ba- or Sr-rich phases were observed in the nearly pure metal matrix of each liquid metal, confirming the reduction of Ba and Sr into the liquid metal electrodes (Figures 2 and 3). Upon solidification, electropositive Ba and Sr formed intermetallic compounds in each liquid metal that can be found in their respective binary phase diagrams, for example, the Ba–Sb (25–75 mol %) phase as $BaSb_3$ and Sr–Bi (22–78 mol %) as $SrBi_3$. However, the composition of the Ba–Bi phase (38–62 mol %) was substantially different from the expected $BaBi_3$ compound, indicating the formation of a ternary Ba–Li–Bi compound and the codeposition of Li. Recently, Ojwang and Bobev identified a new ternary $Ba_7Li_{11}Bi_{10}$ compound, which has a Ba/Bi molar ratio of 41:59, similar to the ratio of 38:62 noted in this work by SEM–EDS.[18]

The codeposition of Li was also observed from the unidentified regions in the SEM–EDS images beyond the instrument capability. For example, both Sr and Bi are depleted in a distinct dark region in the Sr–Bi image (Figure 3) due to the presence of a light element Li, which is confirmed via ICP-AES analysis in the following section.

Composition of Electrolysis Products in Pure Liquid Metal Electrodes. The composition of electrolysis products (X = Ba, Sr, Li, and K) in the liquid metal electrodes was analyzed using ICP-AES for each electrolyte (Table 1). The

Table 1. Composition of Electrolysis Products in Liquid Metals at a Specific Charge of 200 C g^{-1} in the Ternary LiCl–KCl–$BaCl_2$/$SrCl_2$ Electrolyte at 500 or 650 °C for Sb by ICP-AES and the Estimated Faradaic Efficiency

electrolysis products in liquid metal electrodes				
LiCl–KCl–$BaCl_2$ electrolyte				
liquid metal	Ba (wt %)	Li (wt %)	K (wt %)	Faradaic eff. (%)
Sb	7.46 (±0.30)	0.36 (±0.01)	0.45 (±0.02)	82.9 (±0.4)
Bi	8.33 (±0.33)	0.25 (±0.01)	0.31 (±0.01)	79.5 (±0.5)
Sn	6.14 (±0.25)	0.41 (±0.02)	2.01 (±0.08)	96.1 (±0.3)
Pb	6.12 (±0.24)	0.46 (±0.02)	0.52 (±0.02)	81.1 (±0.3)
LiCl–KCl–$SrCl_2$ electrolyte				
	Sr (wt %)	Li (wt %)	K (wt %)	Faradaic eff. (%)
Sb	3.06 (±0.12)	0.43 (±0.02)	0.16 (±0.01)	65.8 (±0.1)
Bi	2.53 (±0.10)	0.33 (±0.01)	0.20 (±0.01)	53.2 (±0.1)
Sn	2.22 (±0.09)	0.45 (±0.02)	0.14 (±0.01)	57.5 (±0.1)
Pb	2.04 (±0.08)	0.51 (±0.02)	0.03 (±0.00)	58.1 (±0.1)

mass of each electrolysis product (m_X) was then converted to the charge passed (Q_X) using Faraday's law:

$$Q_X = \left(\frac{m_X n F}{M_X}\right) \quad (1)$$

where n is the number of electrons consumed in the reaction ($n = 1$ for Li and K; $n = 2$ for Ba and Sr) and M_X is the molar mass. Knowing the total amount of charge passed into the electrode ($Q_{exp} = 540$ C), the Faradaic efficiency was estimated according to:

https://dx.doi.org/10.1021/acssuschemeng.0c04249
ACS Sustainable Chem. Eng. XXXX, XXX, XXX–XXX

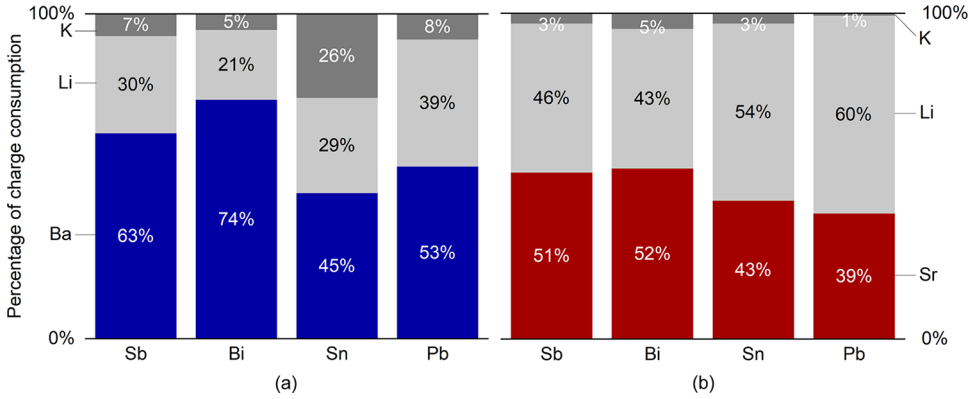

Figure 4. Percentage of charge consumed by each cation for deposition into each liquid metal (Sb, Bi, Sn, and Pb) in (a) LiCl–KCl–$BaCl_2$ and (b) LiCl–KCl–$SrCl_2$ electrolytes, based on chemical analysis by ICP-AES.

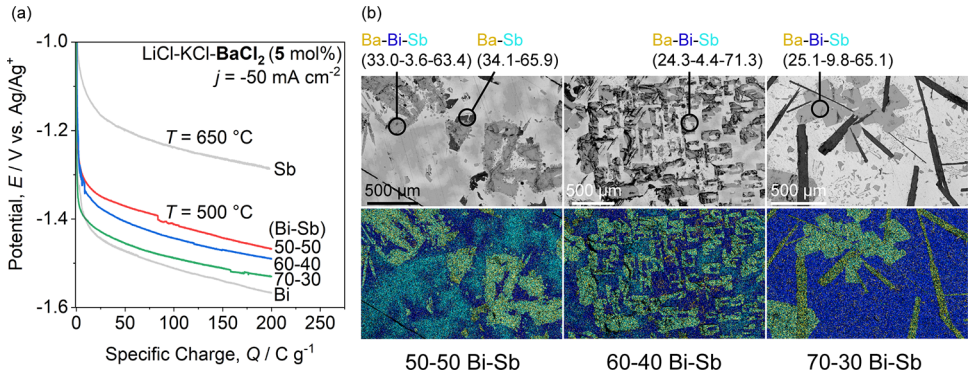

Figure 5. (a) Electrode potential of liquid Bi–Sb alloys (vs Ag/Ag^+) in LiCl–KCl–$BaCl_2$ during electrolysis at $j = -50$ mA cm^{-2} and 500 °C and (b) SEM and elemental X-ray mapping images after electrolysis (Ba = yellow, Bi = dark blue, and Sb = light blue).

$$\text{Faradaic efficiency (\%)} = \frac{\sum_X Q_X}{Q_{exp}} \times 100 \quad (2)$$

The Faradaic efficiencies from ICP-AES were largely scattered among the electrodes, and substantial loss was evident (Table 1). The primary cause for the low and inconsistent Faradaic efficiency is thought to come from sample preparation when deionized water was used to remove the entrained salt from the electrode surface, resulting in the loss of reactive alkali and alkaline-earth metals to the aqueous solution (e.g., $Li + H_2O \rightarrow LiOH(aq) + 1/2H_2(g)$).[19] Assuming that the loss of each electrolysis product is uniform during the sample preparation, the charge for each electrolysis product (eq 2) was normalized with respect to $\sum_X Q_X$ in order to estimate the percentage of charge for each electrolysis product (Figure 4).

The chemical analysis of electrolysis products confirmed the Ba/Sr recovery by all liquid metal electrodes as well as the codeposition of Li (Figure 4). A greater proportion of charge was consumed by Ba^{2+} ions (45–74%) than Sr^{2+} ions (39–52%) during electrolysis from their respective ternary electrolytes, possibly due to lower activity values of Ba than Sr in the liquid metals. For the liquid Bi and Sb electrodes, a greater percentage of charge was consumed for Ba/Sr deposition than the liquid Sn and Pb electrodes, suggesting their enhanced capability to recover alkaline-earth fission products with less removal of Li and K from molten salts. Despite Ba/Sr having stronger interactions with Sb than Bi, the liquid Bi electrode recovered more Ba and Sr than the Sb electrode. The lower recovery capability of the Sb electrode is thought to come from the higher operating temperature of the Sb electrode (650 °C) that can accelerate side reactions such as the dissolution of Ba and Sr metals into the molten salts.[20]

Recovery of Ba and Sr by Liquid Bi–Sb Alloys. The two metals (Bi and Sb), most effective at recovering Ba/Sr, were combined as liquid alloy electrodes and investigated to further enhance the recovery of Ba and Sr from the LiCl–KCl electrolyte while minimizing Li/K removal. By forming Bi–Sb alloys (50–50, 60–40, and 70–30 mol %), the alloy electrodes take advantage of the strongest interactions of Sb with Ba/Sr (i.e., the largest emf values shown in Figure 1) and low melting temperatures for cell operation at 500 °C.[21] A similar approach was effective in improving the performance of the Li–Sb–Pb liquid metal battery by alloying low-melting Pb with Sb in order to retain the high cell voltage of Sb at 450 °C.[22]

Bi–Sb Alloy Electrodes in LiCl–KCl–$BaCl_2$. The potential curves of the Bi–Sb alloy electrodes at 500 °C were located between those of the liquid Bi and Sb electrodes, which shifted toward that of liquid Bi as the Bi content was increased (Figure 5a). After electrolysis, the liquid metal electrodes evolved into a complex microstructure at room temperature (Figure 5b) with: (i) the preferential segregation of Ba to Sb-rich phases, (ii) a Bi–Sb matrix, and (iii) unidentified regions where Ba, Bi, and Sb are depleted due to the presence of the light element Li (e.g., dark regions in the Bi–Sb (70–30 mol %) alloy shown in the SEM image). The preferential segregation of Ba to Sb-rich phases is thought to originate from the stronger chemical interactions with Sb than Bi, for example, $a_{Ba(in\ Sb)} = 1.5 \times 10^{-16}$ and $a_{Ba(in\ Bi)} = 6.8 \times 10^{-16}$ at 500 °C, $x_{Ba} = 0.05$.[10,12]

https://dx.doi.org/10.1021/acssuschemeng.0c04249
ACS Sustainable Chem. Eng. XXXX, XXX, XXX–XXX

Based on the chemical analysis by ICP-AES (Table 2), the percentage of charge for each electrolysis product was estimated (Figure 6). As the Sb content increased, the percentage of charge increased up to 85% for Ba deposition and decreased down to 13−14% for Li deposition, suggesting the enhanced recovery capability of Bi−Sb alloys compared to pure Bi and Sb. Based upon the increased Ba deposition into Bi−Sb alloys and the preferential segregation of Ba to the Sb-rich phases, it is reasonable to suggest that alloying Sb enhances Ba recovery by utilizing the strong chemical interactions between Ba and Sb at 500 °C.

Table 2. Composition of Electrolysis Products in Liquid Bi−Sb Alloys at a Specific Charge of 200 C g^{-1} in the Ternary LiCl−KCl−$BaCl_2$/$SrCl_2$ Electrolyte at 500 °C by ICP-AES and the Estimated Faradaic Efficiency

electrolysis products in liquid Bi−Sb alloys				
LiCl−KCl−$BaCl_2$ electrolyte				
Bi−Sb alloys (mol %)	Ba (wt %)	Li (wt %)	K (wt %)	Faradaic eff. (%)
50−50	7.11 (±0.284)	0.12 (±0.005)	0.04 (±0.002)	58.6 (±0.4)
60−40	6.33 (±0.253)	0.10 (±0.040)	0.07 (±0.003)	52.3 (±0.3)
70−30	8.95 (±0.358)	0.19 (±0.008)	0.21 (±0.008)	78.8 (±0.6)
LiCl−KCl−$SrCl_2$ electrolyte				
	Sr (wt %)	Li (wt %)	K (wt %)	Faradaic eff. (%)
50−50	2.53 (±0.101)	0.44 (±0.018)	0.30 (±0.012)	61.7 (±0.8)
60−40	2.02 (±0.081)	0.49 (±0.020)	0.71 (±0.028)	65.1 (±0.5)
70−30	1.66 (±0.066)	0.68 (±0.027)	1.24 (±0.050)	81.2 (±0.5)

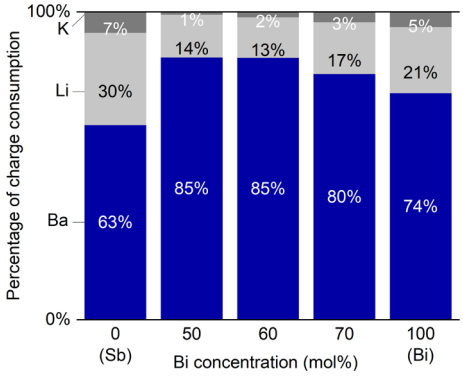

Figure 6. Percentage of charge consumed by each electrolysis product in liquid Bi−Sb alloys (50−50, 60−40, and 70−30 mol %) at 500 °C in LiCl−KCl−$BaCl_2$, compared to liquid Bi and Sb (650 °C).

Bi−Sb Alloy Electrodes in LiCl−KCl−$SrCl_2$. During the initial stage of electrolysis using the Bi−Sb alloy electrodes in LiCl−KCl−$SrCl_2$, the potential curves lie between those of pure Bi and Sb (Figure 7a), similar to the behavior observed in the LiCl−KCl−$BaCl_2$ electrolyte. The Bi−Sb (50−50 mol %) alloy exhibited a smooth potential curve up to 200 C g^{-1}; however, the other Bi−Sb alloys (60−40 and 70−30 mol %) exhibited a steep potential drop during electrolysis, indicating a significant overpotential possibly due to the formation of a solid phase (nucleation overpotential) and transition into complex phase behavior. After electrolysis, the compositions of the electrolysis products in the Bi−Sb alloy electrodes were analyzed by ICP-AES (Table 2).

The microstructure of the Bi−Sb alloys at room temperature confirmed a preferential segregation of Sr to Sb-rich phases (Figure 7b). A distinct Sr-deficient phase was clearly observed in the Bi−Sb (60−40 and 70−30 mol %) electrodes, indicating the codeposition of Li. According to the percentage of charge for each electrolysis product (Figure 8), these two Bi−Sb alloys contained a greater proportion of charge for Li deposition (52−59%) and increased level of K (14−19%),

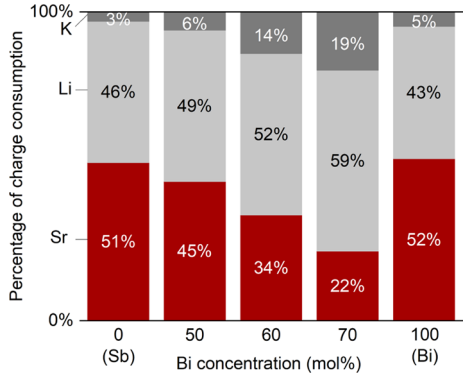

Figure 8. Percentage of charge consumed by each electrolysis product in liquid Bi−Sb alloys (50−50, 60−40, and 70−30 mol %) at 500 °C in LiCl−KCl−$SrCl_2$, compared to liquid Bi and Sb (650 °C).

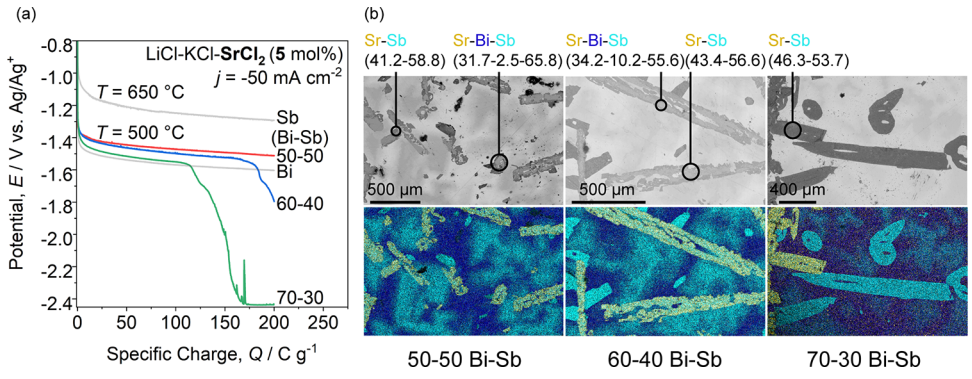

Figure 7. (a) Electrode potential of liquid Bi−Sb alloys (vs Ag/Ag^+) in LiCl−KCl−$SrCl_2$ during constant-current electrolysis at $j = -50$ mA cm^{-2} and 500 °C and (b) SEM and elemental X-ray mapping images after electrolysis (Sr = yellow, Bi = dark blue, and Sb = light blue).

https://dx.doi.org/10.1021/acssuschemeng.0c04249
ACS Sustainable Chem. Eng. XXXX, XXX, XXX−XXX

both of which could be attributed to the large overpotential. Although the increased Sb content in the Bi−Sb alloys enhanced the Sr recovery up to 45% and decreased Li deposition down to 49%, the Sr recovery capability of the liquid Bi−Sb alloys was poor compared to the pure Bi and Sb electrodes, based upon the deposition of less Sr and more Li from the LiCl−KCl−$SrCl_2$ salt.

Overall, the alloying of Sb with Bi improved the recovery capability for Ba recovery; however, it was not effective for Sr recovery possibly due to the complex phase behavior of the multicomponent alloy electrode (e.g., Bi−Sb−Sr−Li) during electrolysis.

CONCLUSIONS

Alkaline-earth metals Ba and Sr were successfully recovered from the LiCl−KCl eutectic electrolyte by electrochemical deposition into liquid metal electrodes by leveraging the strong atomic interactions between alkaline-earth metals and liquid metals. Of the pure liquid metal electrodes investigated, liquid Bi and Sb exhibited greater Ba/Sr recovery than liquid Sn and Pb based on the electrolysis products by ICP-AES. The liquid Bi−Sb alloy electrodes at 500 °C achieved enhanced Ba recovery compared to pure Bi and Sb (650 °C), and the greater the proportion of Sb in the electrode, the greater the Ba recovery. However, the Bi−Sb electrodes were less effective for Sr recovery than either the Bi or Sb electrodes. During electrochemical deposition, Li and K were codeposited into the pure liquid metals and liquid Bi−Sb alloys, possibly leading to a complex phase behavior that influenced Ba/Sr recovery. These comprehensive results indicate that liquid metals and alloys can be used to recover alkaline-earth fission products that accumulate in molten salts during used nuclear fuel recycling processes and minimize additional nuclear waste generated during the recycling process.

AUTHOR INFORMATION

Corresponding Author

Hojong Kim − *Materials Science and Engineering, The Pennsylvania State University, University Park, Pennsylvania 16802, United States;* orcid.org/0000-0002-6247-3474; Phone: 814-865-3117; Email: huk29@psu.edu; Fax: 814-865-2917

Authors

Thomas P. Nigl − *Materials Science and Engineering, The Pennsylvania State University, University Park, Pennsylvania 16802, United States;* orcid.org/0000-0002-0362-9950

Timothy Lichtenstein − *Materials Science and Engineering, The Pennsylvania State University, University Park, Pennsylvania 16802, United States;* orcid.org/0000-0002-4739-9907

Yuran Kong − *Materials Science and Engineering, The Pennsylvania State University, University Park, Pennsylvania 16802, United States;* orcid.org/0000-0001-8641-392X

Complete contact information is available at: https://pubs.acs.org/10.1021/acssuschemeng.0c04249

Notes

The authors declare no competing financial interest.

ACKNOWLEDGMENTS

This work was supported by the US National Science Foundation (grant number: CMMI-1662817) and the US Department of Energy, Office of Nuclear Energy's Nuclear Engineering University Program (Award No. DE-NE0008757).

REFERENCES

(1) *Electrometallurgical Techniques for DOE Spent Fuel Treatment: Final Report*; National Research Council, National Academies Press: Washington, DC, 2000; 1-116.

(2) Williamson, M. A.; Willit, J. L. Pyroprocessing Flowsheets for Recycling Used Nuclear Fuel. *Nucl. Eng. Technol.* **2011**, *43* (4), 329−334.

(3) Bruno, J.; Ewing, R. C. Spent Nuclear Fuel. *Elements* **2006**, *2*, 343−349.

(4) Gutknecht, T. Y.; Fredrickson, G. L.; Utgikar, V. *Thermal Analysis of Surrogate Simulated Molten Salts with Metal Chloride Impurities for Electrorefining Used Nuclear Fuel; INL/EXT-11-23511*; 2012; 1-144.

(5) *Commercial Nuclear Waste: Resuming Licensing of the Yucca Mountain Repository Would Require Rebuilding Capacity at DOE and NRC, Among Other Key Steps; GAO-17-340*; U.S.Government Accountability Office: Washington, DC, 2017; 1-48.

(6) Bale, C. W.; Bélisle, E.; Chartrand, P.; Decterov, S. A.; Eriksson, G.; Gheribi, A. E.; Hack, K.; Jung, I.-H.; Kang, Y.-B.; Melançon, J.; Pelton, A. D.; Petersen, S.; Robelin, C.; Sangster, J.; Spencer, P.; Van Ende, M.-A. FactSage Thermochemical Software and Databases, 2010−2016. *Calphad.* **2016**, *54*, 35−53.

(7) Matsumiya, M.; Takano, M.; Takagi, R.; Fujita, R. Recovery of Ba^{2+} Using Liquid Metallic Cathodes in Molten Chlorides. *J. Nucl. Sci. Technol.* **1998**, *35* (11), 836−839.

(8) Matsumiya, M.; Takagi, R.; Fujita, R. Recovery of Eu^{2+} and Sr^{2+} Using Liquid Metallic Cathodes in Molten NaCl-KCl and KCl System. *J. Nucl. Sci. Technol.* **1997**, *34* (3), 310−317.

(9) Lichtenstein, T.; Nigl, T. P.; Smith, N. D.; Kim, H. Electrochemical Deposition of Alkaline-Earth Elements (Sr and Ba) from LiCl-KCl-$SrCl_2$-$BaCl_2$ Solution Using a Liquid Bismuth Electrode. *Electrochim. Acta* **2018**, *281*, 810−815.

(10) Lichtenstein, T.; Smith, N. D.; Gesualdi, J.; Kumar, K.; Kim, H. Thermodynamic Properties of Barium-Bismuth Alloys Determined by Emf Measurements. *Electrochim. Acta* **2017**, *228*, 628−635.

(11) Smith, N. D.; Lichtenstein, T.; Gesualdi, J.; Kumar, K.; Kim, H. Thermodynamic Properties of Strontium-Bismuth Alloys Determined by Electromotive Force Measurements. *Electrochim. Acta* **2017**, *225*, 584−591.

(12) Lichtenstein, T.; Gesualdi, J.; Nigl, T. P.; Yu, C. T.; Kim, H. Thermodynamic Properties of Barium-Antimony Alloys Determined by Emf Measurements. *Electrochim. Acta* **2017**, *251*, 203−211.

(13) Smith, N. D.; Orabona, N.; Lichtenstein, T.; Gesualdi, J.; Nigl, T. P.; Kim, H. Thermodynamic Properties of Sr-Sb Alloys via Emf Measurements Using Solid CaF_2-SrF_2 Electrolyte. *Electrochim. Acta* **2019**, *305*, 547−554.

(14) Lichtenstein, T.; Gesualdi, J.; Yu, C.-T.; Kim, H. Thermochemical Properties and Phase Transitions of Ba−Sn Alloys from Thermal Characterization and Emf Measurements. *J. Alloys Compd.* **2019**, *811*, 151531.

(15) Smith, N. D.; Paz Soldan-Palma, J.; Kong, Y.; Liu, Z.-K.; Kim, H. Thermodynamic Properties of Sr−Sn Alloys via Emf Measurements and Thermal Analysis. *J. Electrochem. Soc.* **2020**, *167*, No. 082508.

(16) Gesualdi, J.; Nigl, T. P.; Lichtenstein, T.; Smith, N. D.; Kim, H. Thermodynamic Properties of Ba-Pb Alloys Determined by Emf Measurements Using Binary CaF_2-BaF_2 Electrolyte. *J. Electrochem. Soc.* **2019**, *166*, D268−D275.

(17) Nigl, T. P.; Lichtenstein, T.; Smith, N. D.; Gesualdi, J.; Kong, Y.; Kim, H. Thermodynamic Properties of Strontium-Lead Alloys

Determined by Electromotive Force Measurements. *J. Electrochem. Soc.* **2018**, *165*, H991−H998.
(18) Ojwang, D. O.; Bobev, S. Synthesis and Structural Characterization of $Ba_7Li_{11}Bi_{10}$ and $AE_4(Li,Tr)_7Pn_6$ (AE = Sr, Ba, Eu; Tr = Ga, In; Pn = Sb, Bi). *Inorganics* **2018**, *6* (4), 109.
(19) Lichtenstein, T.; Nigl, T. P.; Kim, H. Recovery of Alkaline-Earths into Liquid Bi in Ternary LiCl-KCl-$SrCl_2$/$BaCl_2$ Electrolytes at 500 °C. *J. Electrochem. Soc.* **2020**, *167*, 102501.
(20) Dworkin, A. S.; Bronstein, H. R.; Bredig, M. A. Miscibility of Liquid Metals with Salts. VIII. Strontium-Strontium Halide and Barium-Barium Halide Systems. *J. Phys. Chem.* **1968**, *72* (6), 1892−1896.
(21) Feutelais, Y.; Morgant, G.; Didry, J. R.; Schnitter, J. Thermodynamic Evaluation of the System Bismuth-Antimony. *Calphad* **1992**, *16* (2), 111−119.
(22) Wang, K.; Jiang, K.; Chung, B.; Ouchi, T.; Burke, P. J.; Boysen, D. A.; Bradwell, D. J.; Kim, H.; Muecke, U.; Sadoway, D. R. Lithium-Antimony-Lead Liquid Metal Battery for Grid-Level Energy Storage. *Nature* **2014**, *514*, 348−350.

https://dx.doi.org/10.1021/acssuschemeng.0c04249
ACS Sustainable Chem. Eng. XXXX, XXX, XXX−XXX